Two-dimensional monitoring of air pollution in Madrid using a MAXDOAS-2D instrument

David Garcia-Nieto[1, 2], Nuria Benavent[1, 2], Rafael Borge[2] and Alfonso Saiz-Lopez[1]

[1] Department of Atmospheric Chemistry and Climate, Institute of Physical Chemistry Rocasolano, CSIC, Madrid 28006, Spain

[2] Universidad Politécnica de Madrid, UPM, 28006 Madrid, Spain

*Corresponding author: Alfonso Saiz-Lopez (a.saiz@csic.es)

Abstract

Trace gases play a key role in the chemistry of urban atmospheres. Therefore, knowledge about their spatial distribution is needed to fully characterize air quality in urban areas. Using a new Multi-AXis Differential Optical Absorption Spectroscopy (MAXDOAS)-2D instrument, along with an inversion algorithm (bePRO), we report the first two-dimensional maps of nitrogen dioxide (NO_2) and nitrous acid (HONO) concentrations in the city of Madrid, Spain. Measurements were made during two months (May 6 –July 5 2019) and peak mixing ratios of 12 ppbv and 0.7 ppbv for NO_2 and HONO, respectively, were observed in the early morning in the southern part of the downtown area. We found good general agreement between the MAXDOAS-2D mesoscale observations -which provide a typical spatial range of a few kilometers- and the in-situ measurements provided by Madrid´s air quality monitoring stations. In addition to vertical profiles, we studied the horizontal gradients of NO_2 in the surface

layer by applying the different horizontal light path lengths in the two spectral regions included in the NO_2 spectral analysis: ultraviolet (UV, at 360 nm) and visible (VIS, 477 nm). We also investigate the sensitivity of the instrument to infer vertically-distributed information on aerosol extinction coefficients and discuss possible future ways to improve the retrievals. The retrieval of two-dimensional distributions of trace gas concentrations reported here provides valuable spatial information for the study of air quality in the city of Madrid.

1 Introduction

Air pollution in urban areas has become a concern in our society because it represents a major risk to human health and the environment (WHO, 2019). Air quality is often expressed as the state of air pollution in terms of gaseous pollutant concentrations as well as size and number of particulate matter that may affect human health, ecosystems and climate (Monks et al., 2009). Integral understanding of air pollution requires knowledge about the sources, pollutants, chemical composition and spatial distribution, and their transport phenomena in the atmosphere (EEA, 2019).

Madrid, Spain, has suffered from severe air pollution in recent years, with episodes of large nitrogen dioxide (NO_2) and ozone (O_3) concentrations. In an effort to control and reduce high pollution events, the local government has enforced some traffic restriction measures (Izquierdo et al., 2020) and has set up several in-situ air quality monitoring stations over the city's metropolitan area. These in-situ instruments -as of today- cannot measure some important trace gases present in the atmosphere and their values are only representative of the immediate surrounding of the instruments and at surface level. There is therefore a need for mesoscale analysis (both in horizontal and vertical, in the order of 10 km) of urban air pollution that could

complement the in-situ measurements. With this aim, we have deployed a Multi AXis Differential Optical Absorption Spectroscopy (MAXDOAS) instrument for air pollution measurements in Madrid. MAXDOAS is a widely used technique for the detection of trace gases in the atmosphere and it is based on the wavelength dependent absorption of scattered sunlight by atmospheric constituents (Platt and Stutz, 2008). In addition to routinely monitored species such as NO_2 and O_3, MAXDOAS provides mesoscale measurements of other trace gases that are relevant to understand atmospheric chemistry, such as nitrous acid (HONO), formaldehyde (HCHO) or glyoxal (CHOCHO). Over the past few years, we have reported trace gas measurements in Madrid using the MAXDOAS technique (Wang et al., 2016; Garcia-Nieto et al., 2018; Benavent et al., 2019) as well as pollutants trend analysis and chemical transport modelling (Borge et al., 2018; Cuevas et al., 2014; Saiz-Lopez et al., 2017).

For this work, a new two-dimensional MAXDOAS instrument (which will be described in Sect. 3 and will be hereafter referred to as MAXDOAS-2D) has been built, tested and set up to take continuous measurements in Madrid. This instrument represents a follow-up development to our previous one-dimensional instrument (MAXDOAS-1D, see Wang et al., 2016) that incorporates the capability of moving in the azimuthal dimension, therefore allowing the collection of spectra pointing at any angular direction. This additional capability allows the measurement of both the horizontal and vertical trace gas (e.g. NO_2) distribution throughout the city and in turn the generation of two-dimensional maps of trace gas concentrations. Several works using two-dimensional MAXDOAS instruments have been carried out in recent years (e.g. Ortega et al., 2015, Yang et al., 2019, Schreier et al., 2020, Dimitropolou et al., 2020). These studies were mostly focused on mapping the NO_2 distribution in urban environments and assessing its role for air quality monitoring.

Here we present two months of MAXDOAS-2D measurements of scattered sunlight spectra. The measurements were taken from May 6, 2019 to July 5, 2019, with focus on the evaluation of NO_2 vertical concentration profiles and the characterization of horizontal light path lengths. We also provide the retrieval of HONO as an example of the potential of the MAXDOAS-2D to provide spatial information also on other trace gases relevant to urban atmospheric chemistry. An assessment of the relation between the MAXDOAS data and the in-situ measurements of NO_2 in the city was carried out. Sect. 2 provides details of the DOAS technique while Sect. 3 describes the experimental setup. The inversion methods and the atmospheric parameters chosen for the analysis are detailed in Sect. 4. The two-dimensional NO_2 and HONO distributions, an evaluation of the light path geometries, along with their relative probabilities, and an assessment of horizontal mixing ratio gradients near the surface are discussed in Sect. 5.

2 Brief introduction to the DOAS method

The DOAS basic idea is described by the Beer-Lambert law, which models the exponential attenuation of spectral irradiance when it traverses a certain sample that contains some absorbers:

$$I(\lambda, L) = I_0(\lambda)\, exp\left(-\sum_i \int_0^L \sigma_i(\lambda)\, \rho_i(s) ds\right) \quad (1)$$

where λ is wavelength, σ_i and ρ_i stand for -respectively- the absorption cross section and concentration of a given absorber i along the path, while the pair I_0 and I represent the spectral irradiances at the beginning and end of the process at study.

105 The absorption processes are integrated over the photon paths (with infinitesimal
106 path ds) and summed over every present absorber (Platt and Stutz, 2008).

107

108 Specifically, the MAXDOAS technique is based on the study of the differential
109 spectral absorption structures that are produced in the measured scattered sunlight
110 spectra (Hönninger et al., 2004; Plane and Saiz-Lopez, 2006; Platt and Stutz, 2008). The
111 main principle is based on identifying the narrowband absorption features within the
112 measured optical density taking out the broadband optical density, mainly generated
113 by Rayleigh and Mie scattering, as well as by instrumental effects. On the other hand,
114 an analogous process is done on the trace gases absorption cross sections by means
115 of filtering out the broadband spectral features, hence producing the so-called
116 differential absorption cross sections, which are unique for each trace gas, acting as
117 their "fingerprints" and therefore enabling their specific detection.

118

119 For MAXDOAS, I_0 stands for the solar spectrum (known as the Fraunhofer
120 spectrum, with no Earth atmospheric absorptions), while I represents the recorded
121 ground-based spectrum, which includes all the absorption and scattering processes.
122 However, and since the actual photon path is difficult to determine with accuracy (see
123 Sect. 4), the MAXDOAS calculations are done using relative absorptions between two
124 different optical paths: a zenith spectrum -that contains less absorptions and is
125 assumed as a reference spectrum- and other spectrum pointing to a given elevation
126 angle. Therefore, the direct product of the method is the differential slant column
127 density (DSCD), which can be defined as the difference in the integrated concentration
128 of a given absorber between the two selected pointing directions (more details about
129 the numerical procedure that lies behind can be found in Honninger et al., 2004, Plane
130 and Saiz-Lopez, 2006 and Platt and Stutz, 2008). Finally, these DSCDs are used as the
131 main input for the profile retrieval algorithms, which simulate the state of the

atmosphere with the purpose of reproducing the measured DSCDs. This final step yields the optimal vertical concentration profiles.

3 Experimental

Briefly, MAXDOAS-1D instruments consist of a light collector attached to a stepper motor that scans the atmosphere at different Viewing Elevation Angles (VEA, see Fig. 1). The main feature added to the MAXDOAS-2D instrument is an additional stepper motor for the azimuthal movement, hence allowing the light collector to freely point to any angular direction in the atmosphere. This allows the evaluation of trace gases absorptions for different Viewing Azimuth Angles (VAAs) (Fig. 1).

3.1 MAXDOAS-2D description

A MAXDOAS-2D instrument (Fig. 2) was built by the Atmospheric Chemistry and Climate group at the Institute of Physical Chemistry Rocasolano (IQFRCSIC). Its main elements are based on our previous MAXDOAS-1D instrument: a light collector attached to a stepper motor, along with a focusing lens (80 mm focal length) are responsible for collecting the scattered sunlight. An Ocean Optics, SMA 905 optical fiber of 1-meter length conducts the light through an Ocean Optics, HR4000 spectrometer (which incorporates a linear silicon CCD array as detector). The spectrometer wavelength ranges roughly from 300 nm to 500 nm and offers an estimated spectral resolution (full width at half maximum) of about 0.5 nm. An additional stepper motor was included for azimuthal movement. The instrument incorporates all its components in an outdoor unit. Therefore, to maintain the spectrometer temperature as steady as possible -for both mechanical and wavelength

calibration purposes- a Peltier cell was included. Additionally, an UPS device provides the power supply and eliminates possible strong power peaks. Two webcams take pictures of the cloud cover at each VAA, and monitor the instrument itself. The instrument is autonomous and it runs on a homemade Java software. This software controls the movement, the spectra collection and recording, the surrounding accessories and automatically keeps it continuously measuring as long as the Sun is over the horizon.

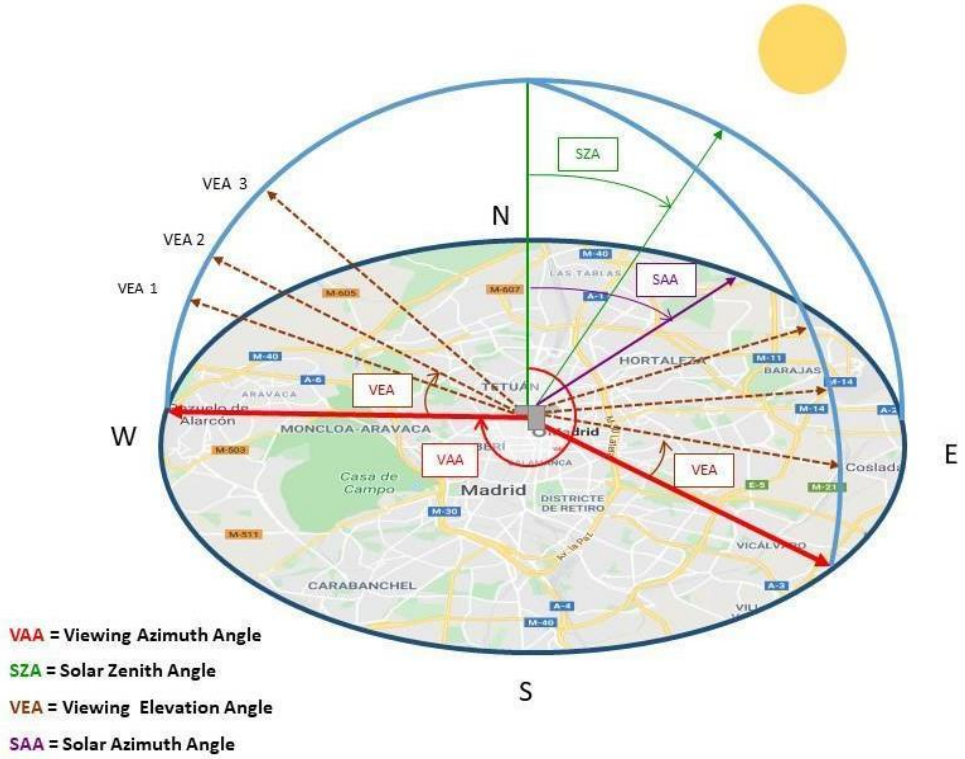

Figure 1. MAXDOAS-2D geometry diagram, the background of this picture represents the Madrid city center taken from Google Maps.

3.2 Location

The MAXDOAS-2D instrument is located at the main campus of the Spanish National Research Council (CSIC) in Madrid, Spain. It is placed on the roof of the Instituto de Ciencias Agrarias (ICA) at a latitude of 40.4419° N and a longitude of 3.6875° W. The height of the building is approximately 70 m above ground level. This location in downtown Madrid can be classified as an urban site, with the usual weather of continental areas at mid-latitudes (i.e. hot and dry summers and cold winters), with prevalence of clear sky days during the year. NO_2 typically presents strong spatial concentration gradients in urban areas and traffic hot-spots have been reported in Madrid (Borge et al., 2016). This makes it difficult to clearly predict how NO_2 will be distributed, i.e., there is not a clear azimuthal direction preference for higher NO_2 at a certain time. However, mesoscale simulations suggest that higher NO_2 mixing ratios can be expected in the southern part of Madrid, considering population distribution and commuting patterns (Picornell et al., 2019).

Due to some obstacles that blocked a clear view in some of the VAAs, a small aluminum tower was built to overcome the viewing obstacles and the MAXDOAS-2D instrument was fixed on top of it (see Fig. 2). Once the instrument was set up, we aligned it for both angular movements -azimuthal and zenithal- with respect to the geographical north and the local horizontal (i.e. perpendicular to the gravitational plumb), respectively. This process was performed in two steps: first, the light collector was coarsely oriented using levels and a compass. Then, the alignment was refined doing a vertical scan of the Sun (which has a very well-known position vector) and its angular surroundings at several different times of a clear sky day. The angular differences between the measurements and the center of intensity of the registered spectra (a similar approach was done in Ortega et al., 2015) were estimated and the associated correction applied to the instrument.

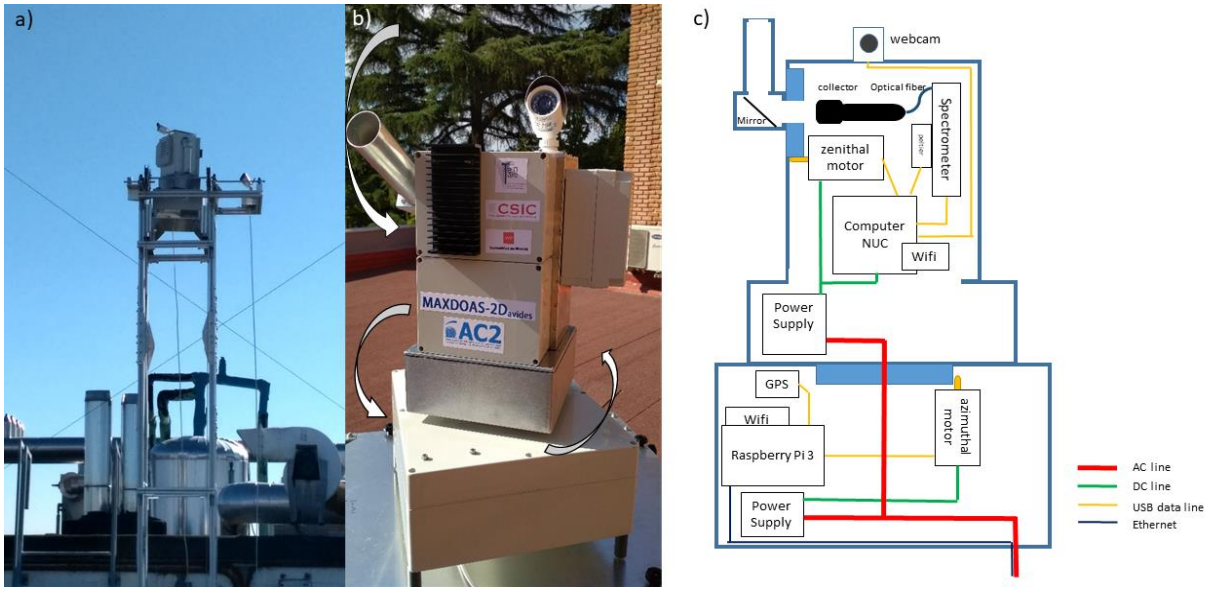

Figure 2. a) Aluminum tower with the instrument installed on top of it; b) MAXDOAS-2D instrument; c) MAXDOAS-2D scheme.

3.3 Measurements set up

In order to sample and analyze a representative portion of the atmosphere over Madrid, selected angular directions were chosen. Starting at a VAA of 0º (pointing to the north), the MAXDOAS-2D rotated clockwise using steps of 20º in azimuth. In each azimuth direction, the ensuing VEA vector was used: 1, 2, 3, 5, 10, 30 and 90 degrees. Therefore, an entire azimuthal lap was completed when the light collector was back again at VAA of 0 degrees.

For every measured spectrum, the spectrometer was able to correct for both electronic offset and dark current effects. Other important parameters for the measurements such as the integration time and the number of scans taken in each angular direction were automatically calculated. More specifically, for this study we set the goal of completing an azimuthal lap in approximately one hour (mainly for an

easier interpretation of the results and for the subsequent comparison with in-situ instruments of Madrid´s air quality monitoring network). Hence, we chose 24 seconds as the maximum exposure time in each angular combination.

The main advantage of this set-up is that we can observe the daily NO_2 variability over the entire city with a moderate temporal resolution (1-hour). The main disadvantage is that observations for each VAAs averaged over such a short integration period may be affected by microscale phenomena. Nonetheless, NO_2 concentration gradients are particularly strong in space (Borge et al., 2016). Therefore, this time resolution may be well suited to characterize both the azimuthal and the horizontal gradients of NO_2.

4 Analysis methods

The absorptions of the molecular oxygen dimer (O_4) and NO_2 were measured for the entire campaign and for two spectral windows: 352-387 nm (UV region) and 438-487 nm (VIS region). The analysis settings applied for the UV and VIS regions are summarized in Tables 1 and 2, respectively. These configurations mainly follow those used in Wagner et al., 2019.

Table 1. DOAS spectral settings for the retrieval of O_4 and NO_2 in the UV.

Parameter	Value
Fitting window	352-387 nm

Wavelength calibration	Based on reference solar atlas (Chance and Kurucz, 2010)
Zenith reference	Scan
Polynomial Order	5
Intensity Offset	Order 2
Shift	The measured spectra and Ring were allowed to shift and stretch (order 1) in wavelength.

Molecule	**Cross section**
O_4	293 K (Thalman and Volkamer, 2013)
NO_2	298 K (Vandaele et al., 1998)
O_3 a	273 K (Serdyuchenko et al., 2014)
O_3 b	223 K (Serdyuchenko et al., 2014)
HCHO	297 K (Meller and Moortgat, 2000)
HONO	296 K (Stutz et al., 2000)
Ring_a	Calculated by QDOAS
Ring_b	Ring_a spectrum multiplied by λ^{-4}

238

239 **Table 2.** DOAS spectral settings for the retrieval of O_4 and NO_2 in the VIS.

Parameter	Value
Fitting window	438-487 nm
Wavelength calibration	Based on reference solar atlas (Chance and Kurucz, 2010)
Zenith reference	Scan
Polynomial order	5
Intensity offset	Order 2
Shift	The measured spectra and Ring were allowed to shift and stretch (order 1) in wavelength.
Molecule	**Cross section**
O_4	293 K (Thalman and Volkamer, 2013)
NO_2	298 K (Vandaele et al., 1998)
O_3 a	273 K (Serdyuchenko et al., 2014)
O_3 b	223 K (Serdyuchenko et al., 2014)
H_2O	296 K (Rothman et al., 2010)
Glyoxal	296 K (Volkamer et al., 2005)
Ring_a	Calculated by QDOAS

Ring_b	Ring_a spectrum multiplied by λ^{-4}

The selected differential absorption cross sections -along with the spectral window and parameters included in Tables 1 and 2- were adjusted to the measured differential optical density using the QDOAS spectral fitting software (http://uv-vis.aeronomie.be/software/QDOAS/). Figure 3 shows examples of spectral detection of O_4 and NO_2 for both the UV and VIS regions.

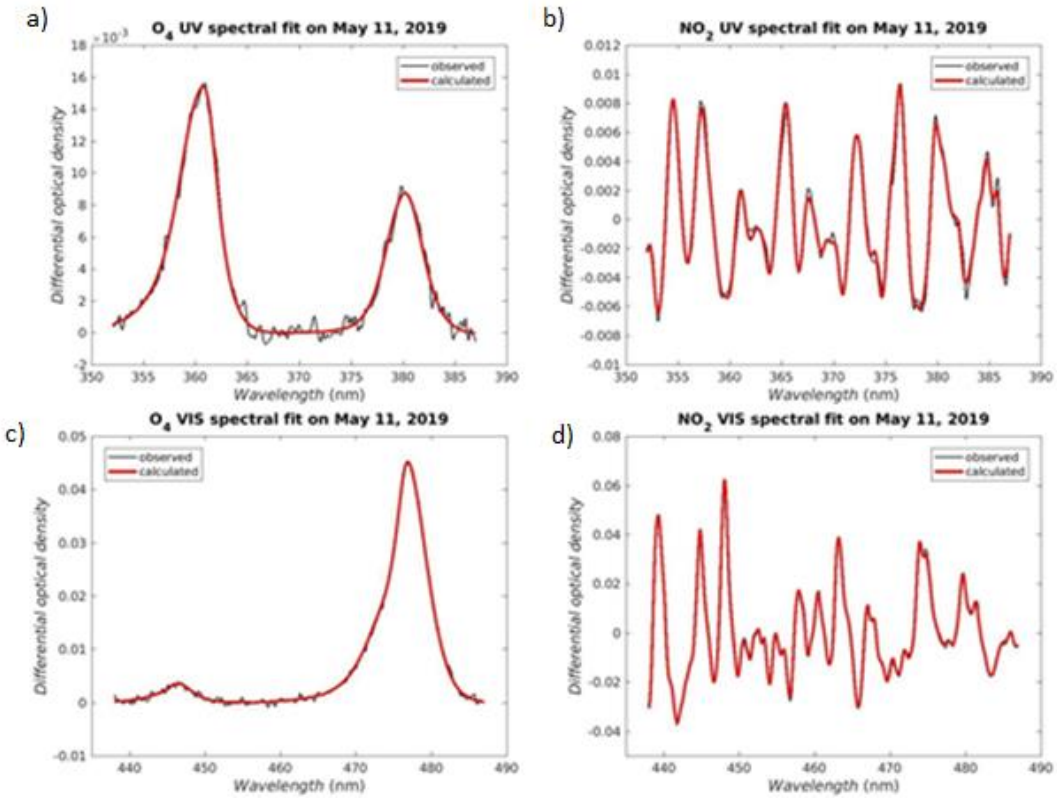

Figure 3. Spectral detection of O_4 (a) and (c) and NO_2 (b) and (d), red lines represent the calculated optical densities and black lines are the measured optical densities. The viewing geometry of each detection was: (a) VEA 2° and SZA 26.4°; (b) VEA 3° and SZA 24.7°; (c) VEA 1° and SZA 22.6° and (d) VEA 1° and SZA 48.7°.

253 **4.1 Cloud-screening and quality filtering**

254

255 The algorithms for MAXDOAS retrievals of trace gas vertical profiles are based
256 on estimating the light paths (along with their corresponding scattering probability). A
257 significant cloud cover could noticeably impact the calculations, mainly because of
258 multiple scattering effects, adding large uncertainties to the retrieval process. For this
259 reason, the set of measured spectra was cloud-screened using the cloud-free AERosol
260 RObotic NETwork (AERONET) database. The AERONET databases are reported with
261 three quality levels, in particular, we used the Level 2.0 (cloud-screened and quality-
262 assured) database provided by the AERONET instrument in Madrid. This information
263 is combined with the photos taken by the camera installed on the MAXDOAS. As
264 mentioned in Sect. 3.1, this webcam points at the same azimuthal direction as the light
265 collector. We estimated the cloud cover using a code that gets the RGB coordinates -
266 the three chromatists of the blue, green and red- and it changes them into LCh
267 coordinates -L indicates lightness, C represents chroma and h is the hue angle. Based
268 on criteria of luminosity, colour and saturation, the code estimates the cloud index
269 (percentage of estimated cloud cover in a given azimuthal sky view). Filtering out
270 cloudy skies with precision is rather challenging, therefore we established a threshold
271 to get as many clear sky views as possible. In order to do that, we first crossed our
272 measured DSCDs with the AERONET 2.0 database, and subsequently, using the photos,
273 we discarded the cycles taken with an estimated cloud index higher than 40 %.

274 In addition to cloud screening, several other quality filters were applied to the
275 DSCDs: firstly, every DSCD that yielded either a relative uncertainty larger than 1 or a
276 residual root mean square (RMS) higher than 0.01 (in optical density units) was
277 rejected. After that, we estimated the DSCDs detection limit for a given trace gas as
278 the ratio of the residual RMS (in optical density units) associated to each DSCD and the
279 maximum value of the differential cross section of that trace gas. Then, we discarded
280 the DSCDs that had an absolute value lower than twice the derived detection limit (a

similar approach was carried out in Peters et al., 2012). Finally, we used the daily plus/minus three standard deviation criterion that AERONET applies for its cloud-filtered data, keeping the DSCD that falls within plus/minus three standard deviations from each daily mean.

4.2 Inversion algorithm and vertical profiles

An inversion algorithm method is applied to the measured DSCDs to estimate the light paths and subsequently derive the trace gas vertical concentration profile. For this work we have used the bePRO inversion algorithm (Clémer et al., 2010). The original calculation was built based on the Optimal Estimation Method (OEM; Rodgers, 2000) and it comprises two steps: first, the light paths and the vertical profiles of irradiance extinction are calculated using the O_4 DSCDs; then, the target trace gas vertical concentration profile is retrieved using the corresponding light paths and measured absorption. In order to do that, bePRO simulates the atmospheric state characterizing several different physical phenomena including pressure and temperature vertical profiles, Rayleigh and Mie scattering events (along with their respective phase functions), the effect of the surface albedo, the light path geometries or the irradiance extinction processes. Once the atmospheric vector state is defined, its combination with a certain vertical concentration profile results in the simulated DSCDs. This vertical profile is iterated until the generated set of simulated DSCDs is optimized with respect to the measured DSCDs so that the residual is minimized. As a result, an optimal vertical profile is obtained when the iteration is finished for each MAXDOAS cycle.

The measured O_4 DSCDs are used to estimate the light paths for each VEA since they are related to the square of the atmospheric O_2 profiles, which are well-known.

This profile is fairly steady during the day and does not heavily depend on chemistry factors. Therefore, the measured O_4 DSCDs can provide information on the irradiance extinction in the atmosphere. This extinction profile is usually associated with the aerosol extinction coefficients and thus, its vertical integration yields the aerosol optical depth (AOD). These aerosol extinction profiles are required to subsequently evaluate trace gas profiles since they strongly affect the relative light paths and hence the concentration profiles derived from them.

Once the light paths are computed, and with the purpose of best simulating the measured DSCDs, a linear analysis process is performed for the measured DSCDs of the target trace gas, yielding the optimal vertical concentration profile. The vertical integration of this concentration profile is called the vertical column density (VCD).

The retrieval consists of an iterative, nonlinear system of equations, and hence there is no unique solution. This means that an a priori profile is needed, both for starting the iterations and to avoid the final solution to be non-realistic (i.e. with no physical meaning). In order to construct these a priori profiles we used exponentially decreasing curves as follows:

$$ap\ (z) = \frac{VC_i}{sh} exp\ \left(\frac{-z}{sh}\right) \quad (2)$$

where $ap\ (z)$ is the a priori vertical profile at a certain altitude z, VC_i is the vertical integration of the profile for the MAXDOAS cycle *i* and *sh* is the scaling height constant. We used 0.5 km as the scaling height constant for all the a priori profiles (Hendrick et al., 2014). Regarding the VC, we assumed an AOD of 0.05 for the O_4 retrieval, while for NO_2 we applied the geometrical approximation followed in Hönninger et al., 2004, taking the measured DSCD at VEA 30° for every MAXDOAS

cycle. This approximation assumes that most of the absorption events are located below the scattering height.

With respect to the remaining atmospheric parameters, we chose typical values for urban environments: surface albedo of 0.07, correlation length of 0.4 km and an a priori covariance factor of 1 (see Hendrick et al., 2014). Concerning the vertical grid of the retrievals, we chose the following layers: from the ground to 8 km height we used layers of 200 m thickness. Then, we divided the remaining height, up to 90 km, in levels of 2 km thickness each. We use the air number density vertical profile since it is directly related to the number of O_4 absorptions, and therefore to the O_4 DSCDs. Hence the relative differences, particularly for lower VEAs, between the measured and simulated O_4 DSCDs are usually assigned to aerosol extinction. Note however, as shown below, that uncertainties in the air number density profiles -arising from uncertainties in the values or shape of the temperature and pressure profiles- could also contribute to such differences (Fig. 4).

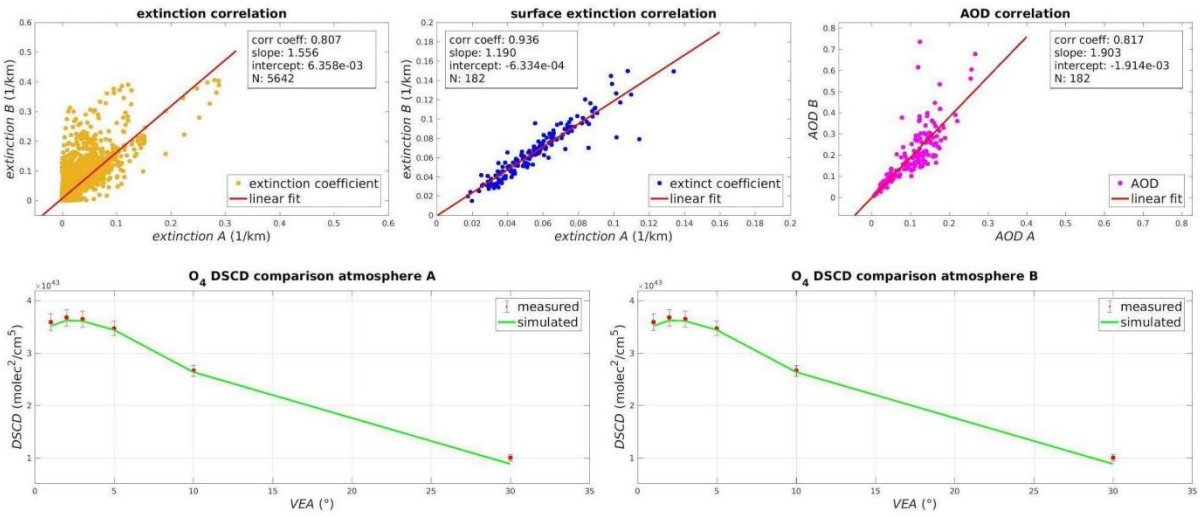

Figure 4. Comparison of retrieved aerosols using two different atmospheric profiles: the US Standard (atmosphere A) and the US Standard adapted to the altitude

above sea level of Madrid (atmosphere B). The comparison was carried out for a clear sky day (May 11, 2019).

Here we compare the simulation of O_4 DSCDs using two different sets of atmospheric profiles: i) the US Standard, and ii) the same profile but interpolating the pressure profile to Madrid´s height above sea level (mean value of 667 m). This means that the temperature profile is assumed to be the same but the pressure profile is shifted less than 10%, so there are no major variations within the profiles. The lower row in Fig. 4 shows that both atmospheric profiles result in almost the same set of simulated O_4 DSCDs, however the aerosol extinction coefficients differ significantly (although less for the surface layer coefficients, defined as the extinction coefficients within the ground layer, between 0 and 200 m height), and consequently, the AOD also varies. From this we infer that:

i) the retrieval is mainly driven by the measured DSCDs, which leaves a relatively low weight for the chosen atmospheric profiles (pressure and temperature). Therefore, we can obtain consistent correlations between the measured and simulated O_4 DSCDs.

ii) we cannot reliably assign the extinction coefficients at each layer to aerosols (especially for atmospheric layers above the surface layer), but rather consider them as irradiance extinction coefficients.

Furthermore, we have assessed the impact of the pressure and temperature profiles choice on the trace gas retrieval. As can be noted in Fig. 5, there is no significant effect coming from this choice on the simulated NO_2 DSCDs. These are

basically the same (and with very good agreement with the measured DSCDs), as well as the derived concentration coefficients and their integration (VCD).

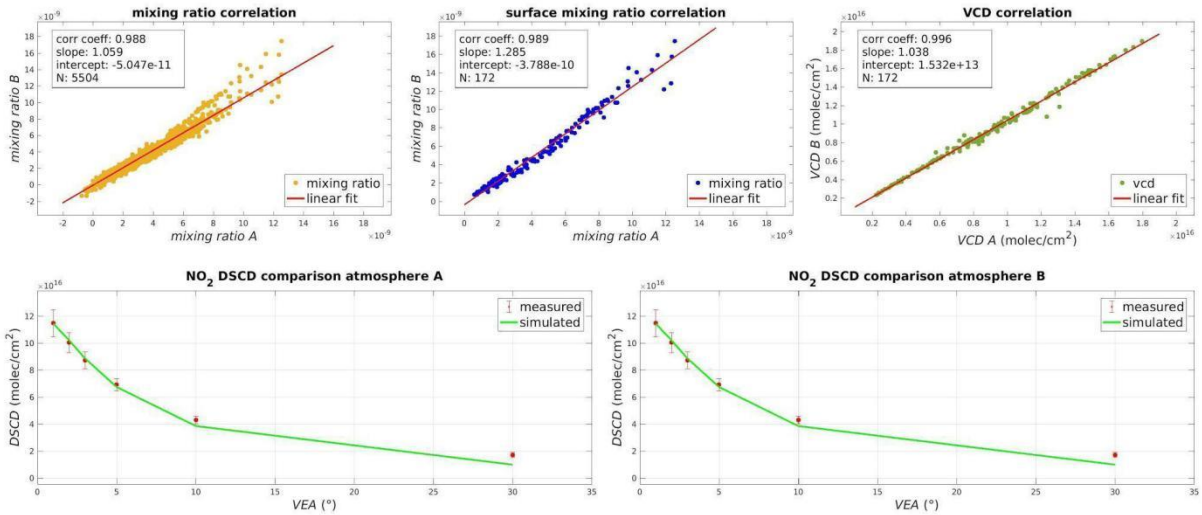

Figure 5. NO_2 retrieval comparison using two different atmospheric profiles: the US Standard (atmosphere A) and the US Standard adapted to the altitude above sea level of Madrid (atmosphere B). The comparison was carried out for a clear sky day (May 11, 2019), considered as representative of the measurement period.

We further evaluated if a similar behavior can be expected for larger variations in the pressure and temperature profiles. We first obtained the average surface temperature and pressure values during the campaign (May-July, 2019). With the inclusion of these values in the retrieval, we found that, within the first 10 km height, the RMS of the relative variations with respect to the standard atmosphere were about 8 %. Although it is a small change, it is indeed not negligible. Nonetheless, when evaluating light paths, the relative changes were below 2%. Therefore, here we use the US Standard atmospheric profiles for the NO_2 retrievals.

Table 3 summarizes the average uncertainties (using one standard deviation for each component) of the retrieval, along with their relative contributions, for the ground layer (0-200 m height). The mean, overall uncertainty for NO_2 in both spectral regions is in the order of 10%.

Table 3. Summary of average uncertainties of the retrieval in both spectral regions.

Variable \ Trace gas	NO_2 UV (%)	NO_2 VIS (%)
Irradiance Extinction	7.7	5.1
DSCD	4.8	3.2
Surface Mixing Ratio	5.0	8.7
Total	10	11

4.3 Estimation of NO_2 horizontal gradients

Making use of the different paths that photons travel through the atmosphere for different wavelengths, we can estimate the horizontal distribution of NO_2. We use the estimated horizontal light paths at two wavelengths, 360.8 nm and 477 nm, for the surface layer (0-200 m height). The different light paths at 360.8 and 477 nm provide information about the horizontal distribution of NO_2 mixing ratios within the surface layer. In order to evaluate these horizontal paths, we have a code that implement the RTM equations based on previous pioneering work (Solomon et al., 1987). These equations yield a vector of scattering events along with their respective probabilities. If we take a VEA of 0 degrees (i.e. horizontal viewing), then the scalar product of such vectors produces the length of the horizontal light path.

We computed this for every MAXDOAS cycle and for both wavelengths, yielding typical -representative- horizontal distances of about 8-10 km for the UV (at 360.8 nm) and between 15-20 km for the VIS window (at 477 nm). The next step follows the "onion-peeling" approach proposed by Ortega et al. 2015 (the strong dependence of scattering with wavelength means that shorter wavelengths result in shorter light paths). We assign the UV (i.e. 360.8 nm) mixing ratios (mr_{uv}) and their expected horizontal paths (d_{uv}) to the first peel (mr_A, meaning zone A). Then the second peel (zone B, mr_B) can be derived as:

$$mr_B = \frac{mr_{vis} \times d_{vis} - mr_{uv} \times d_{uv}}{d_{vis}} \quad (3)$$

Thereby, deriving mixing ratios (mr_a and mr_b) representative of two different horizontal distances for each VAA.

5 Results

5.1 O_4 and NO_2 DSCDs assessment

An estimation of the overall goodness of the profile retrieval comes from the correlation between the measured and simulated DSCDs for the entire campaign (Fig. 6). The fit between the measured and the simulated DSCDs shows correlations (r^2) very close to 1 for both O_4 and NO_2 in the UV and VIS regions.

441 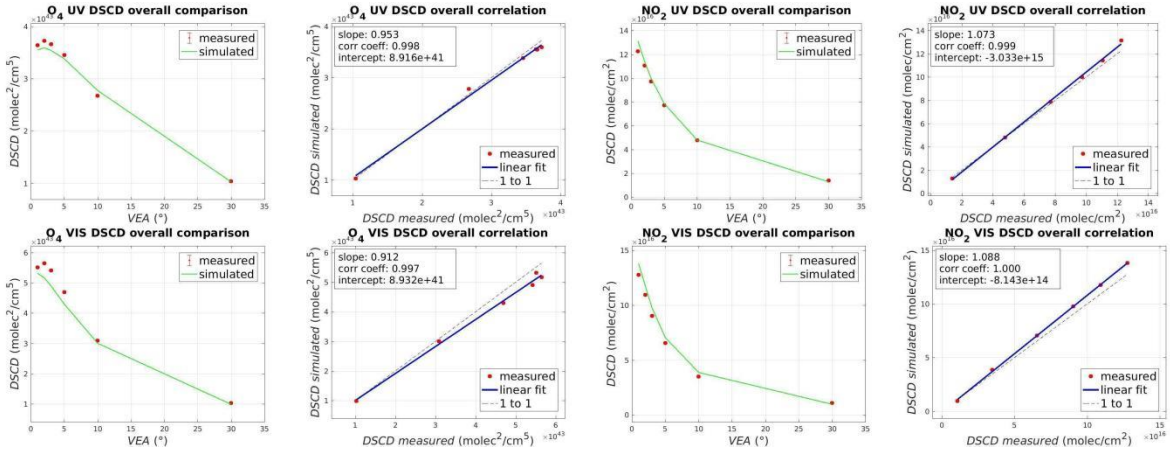

442 **Figure 6**. Comparison between simulated and measured DSCDs of O_4 and NO_2. Red
443 dots represent the measured DSCDs for each VEA, averaged over the entire campaign.

444

445 **5.2 Two-dimensional maps**

446

447 We now combine the VAA and height for each azimuthal cycle of the
448 MAXDOAS-2D to generate a two-dimensional concentration map. Fig. 7 shows an
449 example of the O_4 retrieval in the UV for a given azimuthal cycle. Fig. 7 also shows the
450 comparison and correlation of measured and simulated DSCDs for that azimuthal
451 cycle, along with the evolution of retrieved AOD. The AOD varies between 0.05 and
452 0.18 within this azimuthal cycle (Fig. 7, upper panel). The contour plot shows the
453 irradiance extinction coefficient profiles with maximum values of 0.14 km^{-1} (near the
454 ground and at around 40º VAA) associated with aerosol extinction (see discussion in
455 Sect. 4.2). Note the enhanced extinction at about 2 km height pointing at 50 VAA. This
456 could be due to uplift of particulate matter emitted by traffic (there is a main road at
457 that location) (Carnerero et al., 2018). Further research is needed to better establish
458 the vertical distribution of aerosols in Madrid, and their diurnal evolution.

459

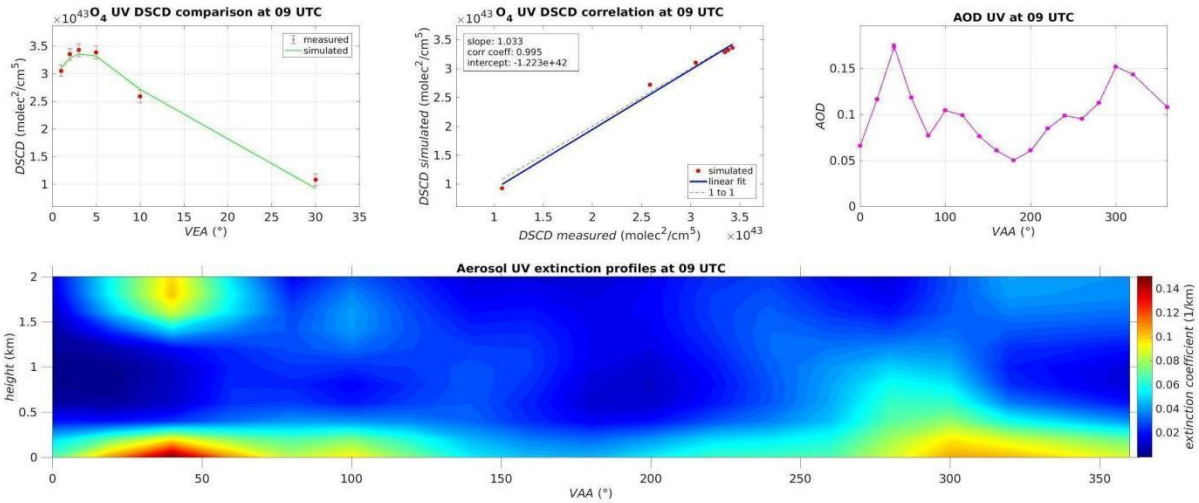

460

461 **Figure 7**. Example of O_4 and AOD retrievals in the UV region at 9 UTC on May
462 11, 2019. These contour plots are smoothed from adjacent VAA data points separated
463 by 20º in order to estimate the azimuthal distribution of the irradiance extinction
464 coefficients over Madrid.

465

466 Figure 8 shows a two-dimensional representation of NO_2 on May 11, 2019 at
467 two different hours (6 UTC and 12 UTC, respectively). Both contour plots show
468 maximum NO_2 values of 12 ppbv at 6 UTC and 8 ppbv at 12 UTC, when the instrument
469 is pointing south (i.e. VAA of 180º). We chose to show this day as an example since it
470 was a clear sky day and yielded NO_2 mixing ratios that were representative of the
471 period of measurements. These values correspond to the layer near the ground and
472 are in good agreement with our previous MAXDOAS observations in Madrid (Garcia-
473 Nieto et al., 2018). The retrieved azimuthal distribution of NO_2 agrees with previous
474 reports that show higher pollution levels in the southern part of Madrid (Picornell et
475 al., 2019). NO_2 VCDs range from $5x10^{15}$ molecules cm^{-2} (at 12 UTC and pointing at 300
476 ° VAA) up to $15x10^{15}$ molecules cm^{-2} (at 12 UTC and pointing at 200º VAA), with an
477 average value of $1x10^{16}$ molecules cm^{-2}. Although there are different NO_X emission
478 rates at both times of the day (6 and 12 UTC), the increase in the boundary layer height

(de la Paz et al., 2016) during the day contribute to the similar values of VCDs at both hours but generally lower surface mixing ratios at 12 UTC.

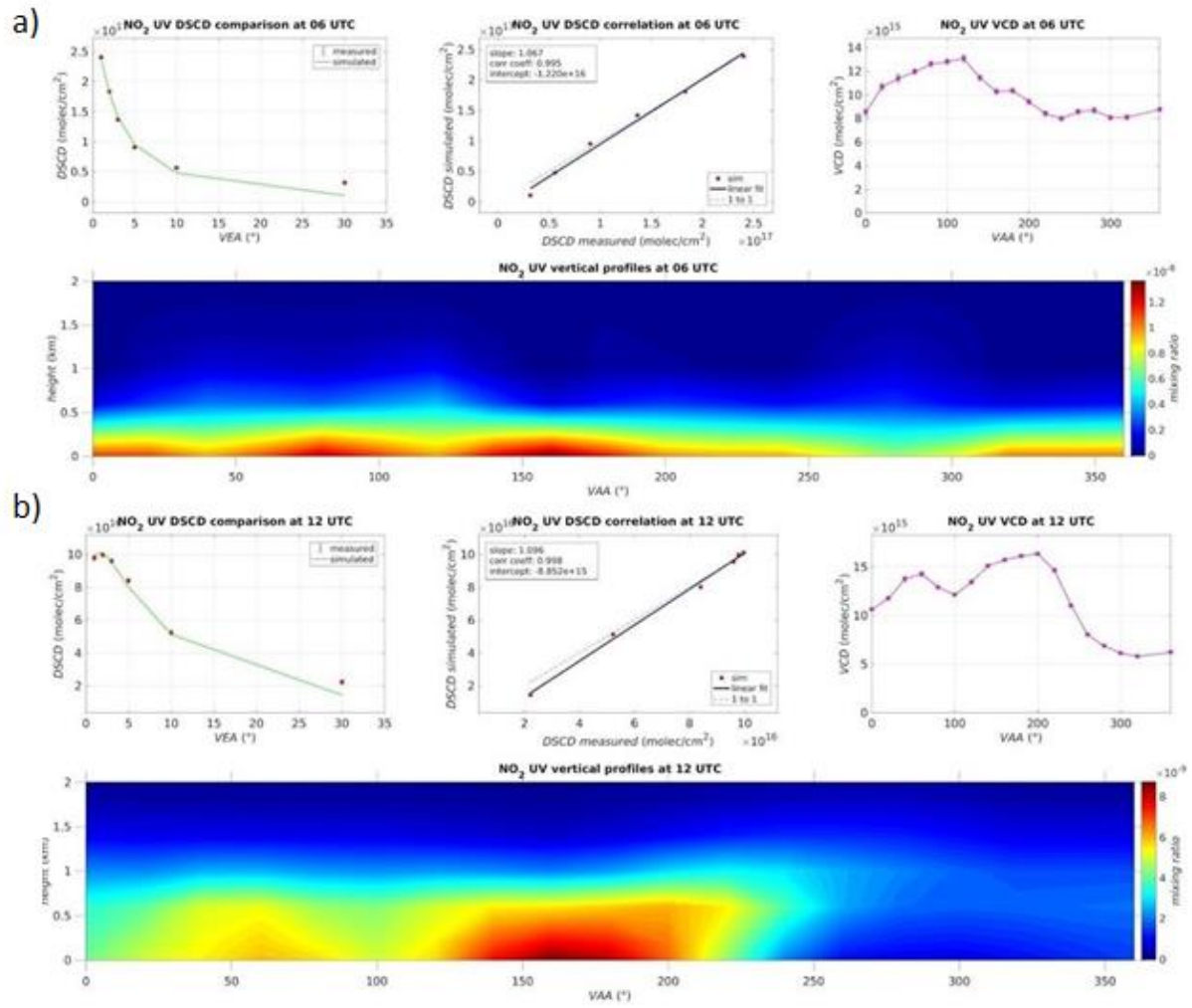

Figure 8. NO_2 vertical distribution retrieved in the UV region at 6 UTC (a) and at 12 UTC (b) on May 11, 2019. These contour plots are smoothed from adjacent VAA data points separated by 20º in order to estimate the azimuthal distribution of NO_2 over Madrid.

We have also analyzed HONO DSCDs using the same DOAS analysis configuration as in Garcia-Nieto et. al., 2018. Figure 9 shows a two-dimensional representation of HONO on May 11, 2019 at 6 UTC. We retrieve surface layer peak values of 0.7 ppbv pointing at 50° of VAA in the early morning, in agreement with

previous studies for HONO in urban environments (see Hendrick et al., 2014; Ryan et al., 2018). The VCDs at 6 UTC range from $6x10^{14}$ to $1.2x10^{15}$ molecule cm^{-2}.

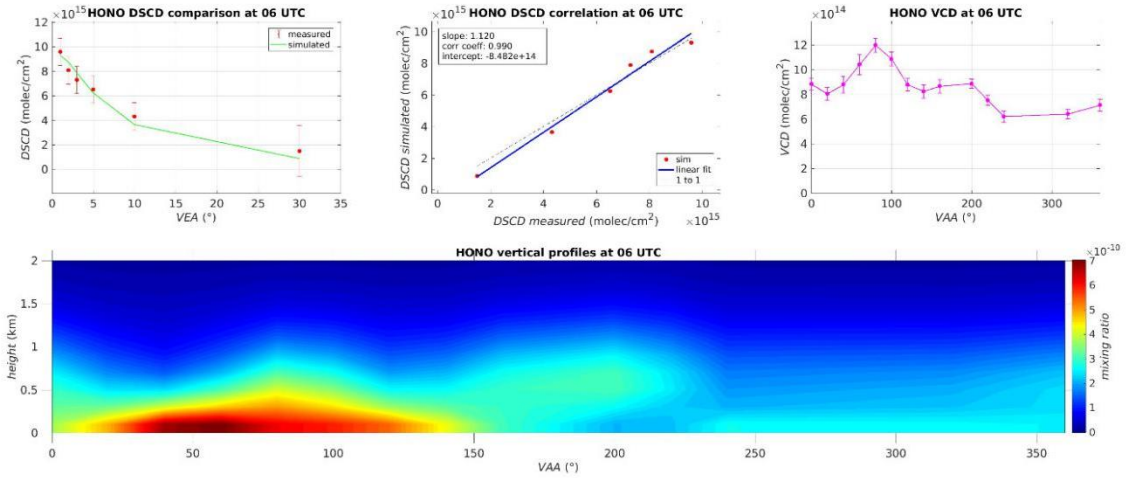

Figure 9. HONO vertical distribution retrieved in the UV region at 6 UTC. These contour plots are smoothed from adjacent VAA data points separated by 20° in order to estimate the azimuthal distribution of HONO over Madrid.

5.3 Horizontal distribution of NO_2

Based on Eq. (3), we derive the horizontal distribution of NO_2 in the surface layer (0-200 m height) using the measured NO_2 DSCDs at a VEA of 1° (which can safely be regarded as almost horizontal viewing, since its mean scattering height typically falls below 200 m height, i.e. within our ground layer). Figure 10 shows an example of surface layer NO_2 mixing ratios over two radial distances horizontally measured from the MAXDOAS-2D instrument (using the UV and the VIS NO_2, respectively, as explained in Section 4.3), located at the center of the plot. The highest mixing ratios occur during the first sunlit hours (7-8 UTC), coincident with the morning peak of NO_X emissions in Madrid (Quassdorff et al., 2016). This early morning peak is followed by a gradual decrease in surface layer NO_2 mixing ratios during the day. Note that NO_2 is

predominantly located in the southern part of the semisphere (VAA from 90º to 270º). In follow up work we will combine the horizontal distribution of NO_2 with a chemical transport model to further understand NO_2 transport dynamics throughout the day.

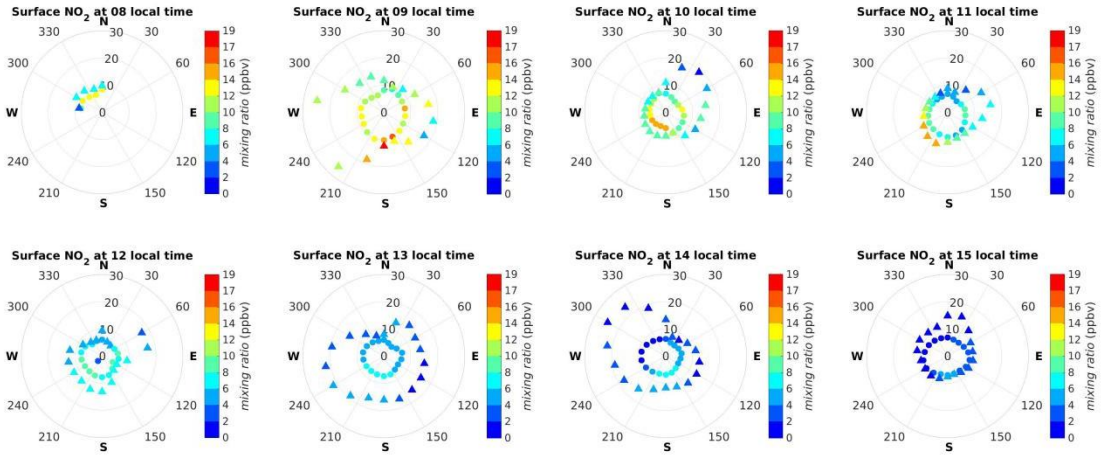

Figure 10. Polar plots of NO_2 within the surface layer (0-200 m height) for May 11, 2019. Please note that these polar plots extend over a direction perpendicular to those shown in Fig. 8. Here, circles are used for the UV (shorter horizontal light path) and triangles for the VIS (larger horizontal light path). Both symbols stand for the mean horizontal light path within the surface layer at each spectral region.

5.4 Correlation with Madrid´s in-situ air quality monitoring stations

We suggest that MAXDOAS-2D mesoscale observations may complement the information provided by the local air quality monitoring network based on reference analytical techniques (according to Directive 2008/50/EC). While air quality monitors of the reference network provide information about ambient concentrations in their specific locations (currently 24 air quality monitoring stations measure NO_2 within the city, see AM, 2019), MAXDOAS-2D observations produce near ground-level

concentrations averaged over the optical path in a given direction. That prevents us from quantitatively comparing both types of observations. Nonetheless, we analyzed their correspondence using the NO_2 concentrations measured by the in-situ instruments throughout the entire city, and the NO_2 mixing ratios within the surface layer derived from our MAXDOAS-2D instrument over the 2-month period (May-June, 2019). For this comparison, we considered the air quality monitoring stations within a distance from the MAXDOAS-2D equal or lower than 10 km (thus remaining 20 air quality monitoring stations). Since this is the typical horizontal light path for the UV region, we decided to include only the NO_2 values retrieved in the UV region for the comparison. Strong gradients between the values measured by the in-situ instruments are typical. Therefore, and considering that we are mainly interested in their temporal correlation with respect to our measurements, we compare both the in-situ NO_2 and surface layer MAXDOAS-2D hourly-averaged data. Note that for the MAXDOAS-2D, this approximately corresponds to averaging the surface layer values for each azimuthal lap, given that each azimuthal lap takes approximately 1 hour to complete.

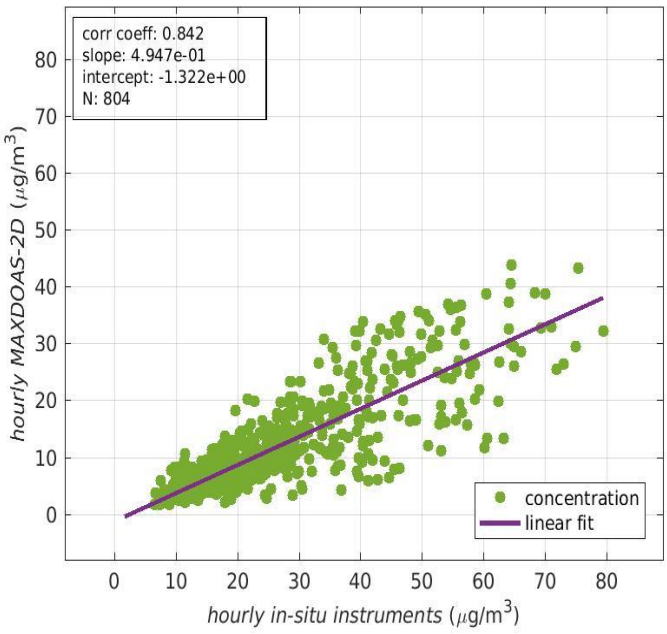

Figure 11. Correlation between in-situ observations from Madrid´s air quality

548 monitoring network and those derived from the MAXDOAS-2D instrument for the
549 surface layer (0-200 m height).

550

551 Despite the different spatial representativeness, Figure 11 shows a reasonably
552 good correlation coefficient of 0.842 between both datasets for the two-month
553 campaign. The slope is lower than 1, this can be explained by the typical NO_2 vertical
554 profiles in urban environments. Simulations performed over Madrid with a high-
555 resolution Eulerian air quality model (Borge et al., 2018) yielded an exponentially
556 decreasing with height NO_2 profile. Therefore, the MAXDOAS-2D mixing ratios, which
557 represent an average across the surface layer (0-200 m height), are not expected to
558 quantitatively match the values of in-situ instruments, located close to the surface
559 (between 0-10 m height). Similar conclusions -and slopes comparable to the one
560 retrieved above- regarding the correlation between in-situ and MAXDOAS instruments
561 can be found in previous works (Schreier et al., 2020; Kramer et al., 2008; Chan et al.,
562 2020). In addition, there is a good temporal correlation between in-situ and
563 MAXDOAS-2D measurements over an extended period of time.

564

565 **6 Summary and Conclusions**

566

567 An analysis of O_4, NO_2 and HONO vertical concentration profiles in the urban
568 atmosphere of Madrid (Spain) has been performed over two months (from May 6 to
569 July 5, 2019). We analyzed the absorptions and derived the corresponding DSCDs for
570 both trace gases in the UV and VIS regions. Then, the corresponding profiles were
571 retrieved using a RTM. In this step, we assessed the impact of different atmospheric
572 profiles (pressure and temperature) in the retrieval results, and found that the set of
573 chosen atmospheric profiles has a small impact on the O_4 retrieval and the estimation
574 of light paths. However, there is a noticeable change in the irradiance extinction

575 profiles, which makes difficult to quantitatively assign extinction due to aerosols,
576 especially in heights above the boundary layer.

577 The overall comparison of measured and simulated trace gas DSCDs showed
578 that they were in very good agreement (with correlation coefficients close to 1),
579 supporting the reliability of the observations. The MAXDOAS-2D instrument provides
580 the first two-dimensional view (in height and VAA) of pollution concentration in the
581 city of Madrid. Exploring one day (May 11, 2019) we compared two hours: the peak
582 rush hour and noon time, obtaining NO_2 maximum values of 12 ppbv and 8 ppbv
583 respectively, both maxima pointing to the south direction. Two-dimensional HONO
584 measurements were also made with mixing ratio peaks of 0.7 ppbv in the early
585 morning, and VCDs ranging from $6x10^{14}$ to $1.2x10^{15}$ molecule cm^{-2}.

586

587 We have also inferred information on the horizontal gradient of NO_2 within the
588 surface layer making use of the strong dependence between wavelengths and light
589 paths across the NO_2 absorption spectrum. The resulting "onion-peeling" figures
590 indicate peak values of NO_2 in the early morning and in the southern section of the city
591 (around 180 º VAA), it resulted in a gradual decrease in NO_2 mixing ratios during the
592 day, maximum values of NO_2 appear in the southern part of the semisphere. Finally,
593 we suggest that the new mesoscale information provided by the MAXDOAS-2D
594 instrument helps in the study of pollution transport dynamics. MAXDOAS-2D and in-
595 situ instruments provide different information, and thus, combining both can improve
596 our understanding of the complex issue of air pollution in the city of Madrid.

597

598 **Author Contribution**

599

A.S-L. devised the research. D.G-N. and N.B. carried out the measurements and analyzed the data. D.G-N., N.B., R.G. and A.S-L. analyzed and interpreted the results. D.G-N. wrote the manuscript with contributions from all co-authors.

Acknowledgements

The authors want to thank Manuel Perez and David Armenteros for technical assistance with the instrument, and David de la Paz for model assistance. This work was supported by the TECNAIRE project ("Técnicas innovadoras para la evaluación y mejora de la calidad del aire urbano") S2013/MAE-2972. We would also like to thank Juan Ramón Moreta González (PI) and his staff for establishing and maintaining the AERONET sites in Madrid used in this investigation. We acknowledge support of the publication fee by the CSIC Open Access Publication Support Initiative through its Unit of Information Resources for Research (URICI)

References

Ayuntamiento de Madrid (AM): Madrid 2016 Annual Air Quality Assessment Report (Calidad del aire Madrid 2019). General Directorate of Sustainability and Environmental Control, Madrid City Council Available online -only Spanish version- at http://www.mambiente.munimadrid.es/opencms/export/sites/default/calaire/Anexos/Memorias/Memoria_2019.pdf, 2019.

624 Benavent, N., Garcia-Nieto, D., Wang, S., & Saiz-Lopez, A.: MAX-DOAS measurements
625 and vertical profiles of glyoxal and formaldehyde in Madrid, Spain. Atmospheric
626 Environment, 199, 357–367, 2019.

627

628 Borge, R., Narros, A., Artínano, B., Yagüe, C., et al.: Assessment of micro- scale spatio-
629 temporal variation of air pollution at an urban hotspot in Madrid (Spain) through an
630 extensive field campaign. Atmos. Environ. 140, 432–445, 2016.

631

632 Borge, R., Santiago, J. L., de la Paz, D., Martín, F., Domingo, J., Valdés, C., Sánchez, B.,
633 Rivas, E., Rozas, M. T., Lázaro, S., Pérez, J., & Fernández, Á.: Application of a short term
634 air quality action plan in Madrid (Spain) under a high-pollution episode - Part II:
635 Assessment from multi-scale modelling. Science of the Total Environment, 635, 1574–
636 1584. https://doi.org/10.1016/j.scitotenv.2018.04.323, 2018.

637

638 Carnerero, C., Pérez, N., Reche, C., Ealo, M., Titos, G., Lee, H.-K., Eun, H.-R., Park, Y.-H.,
639 Dada, L., Paasonen, P., Kerminen, V.-M., Mantilla, E., Escudero, M., Gómez-Moreno, F.
640 J., Alonso-Blanco, E., Coz, E., Saiz-Lopez, A., Temime-Roussel, B., Marchand, N.,
641 Beddows, D. C. S., Harrison, R. M., Petäjä, T., Kulmala, M., Ahn, K.-H., Alastuey, A., and
642 Querol, X.: Vertical and horizontal distribution of regional new particle formation
643 events in Madrid, Atmos. Chem. Phys., 18, 16601–16618,
644 https://doi.org/10.5194/acp-18-16601-2018, 2018.

645

646 Chan, K. L., Wiegner, M., Alberti, C., & Wenig, M.: MAX-DOAS measurements of
647 tropospheric NO_2 and HCHO in Munich and the comparison to OMI and TROPOMI
648 satellite observations. Atmospheric Measurement Techniques Discussions, 2020.

649

Chance, K., Kurucz, R.L.: An improved high-resolution solar reference spectrum for earth's atmosphere measurements in the ultraviolet, visible, and near infrared. J. Quant. Spectrosc. Radiat. Transf.; Special Issue Dedicated to Laurence S. Rothman on the Occasion of his 70th Birthday 111 (9), 1289-1295, 2010.

Clémer, K., Van Roozendael, M., Fayt, C., Hendrick, F., Hermans, C., Pinardi, G., Spurr, R.,Wang, P., De Mazière, M.: Multiple wavelength retrieval of tropospheric aerosol optical properties from MAXDOAS measurements in Beijing. Atmospheric Measurement Techniques 3 (4), 863, 2010.

Cuevas, C., Notario, A., Adame, J. Hilboll, A., Richter, A., Burrows, J.P, Saiz-Lopez, A.: Evolution of NO2 levels in Spain from 1996 to 2012. Sci Rep 4, 5887, 2014.

de la Paz, D., Borge, R., & Martilli, A.: Assessment of a high resolution annual WRF-BEP/CMAQ simulation for the urban area of Madrid (Spain). Atmospheric Environment, 144, 282–296. https://doi.org/10.1016/j.atmosenv.2016.08.082, 2016.

Dimitropoulou, E., Hendrick, F., Pinardi, G., Friedrich, M., Merlaud, A., Tack, F., De Longueville, H., Fayt, C., Hermans, C., Laffineur, Q., Fierens, F., & Van Roozendael, M.: Validation of TROPOMI tropospheric NO_2 columns using dual-scan MAX-DOAS measurements in Uccle, Brussels. Atmospheric Measurement Techniques Discussions, 2020.

European Environment Agency (EEA).: Air quality in Europe – 2019 report. EEA Technical Report No 10/2019. ISBN: 978-92-9480-088-6. Available online at: http://www.eea.europa.eu/publications/air-quality-in-europe-2019., 2019

Hendrick, F., Müller, J.-., Clémer, K.,Wang, P., De Mazière,M., Fayt, C., Gielen, C., Hermans, C., Ma, J., Pinardi, G., Stavrakou, T., Vlemmix, T., Van Roozendael, M.: Four years of ground-based MAX-DOAS observations of HONO and NO_2 in the Beijing area. Atmos. Chemical Physics, 14 (2), 765, 2014.

Garcia-Nieto, D., Benavent, N., Saiz-Lopez, A.: Measurements of atmospheric HONO vertical distribution and temporal evolution in Madrid (Spain) using the MAXDOAS technique. Science of the Total Environment. 643, 957–966, 2018.

Hönninger, G., von Friedeburg, C., Platt, U.: Multi axis differential optical absorption spectroscopy (MAXDOAS). Atmos. Chem. Phys. 4 (1), 231-254, 2004.

Izquierdo, R., García Dos Santos, S., Borge, R., Paz, D. de la, Sarigiannis, D., Gotti, A., & Boldo, E.: Health impact assessment by the implementation of Madrid City air-quality plan in 2020. Environmental Research, 183, 109021, 2020.

Kramer, L. J., Leigh, R. J., Remedios, J. J., & Monks, P. S: Comparison of OMI and ground-based in situ and MAX-DOAS measurements of tropospheric nitrogen dioxide in an urban area. Journal of Geophysical Research Atmospheres, 2008.

Meller, R., Moortgat, G.K.: Temperature dependence of the absorption cross sections of formaldehyde between 223 and 323 K in the wavelength range 225-375 nm. Journal of Geophysical Research: Atmosphere 105, 7089-7101, 2000.

Monks, P. S., Granier, C., Fuzzi, S., Stohl, A., Williams, M. L., Akimoto, H., Amann, M.,Baklanov, A., Baltensperger, U., Bey, I., Blake, N., Blake, R. S., Carslaw, K., Cooper, O. R., Dentener, F., Fowler, D., Fragkou, E., Frost, G. J., Generoso, S., … von Glasow, R.: Atmospheric composition change - global and regional air quality. Atmospheric Environment, 43(33), 5268–5350. https://doi.org/10.1016/j.atmosenv.2009.08.021, 2009.

Ortega, I., Koenig, T., Sinreich, R., Thomson, D., Volkamer, R.: The CU 2-D-MAX-DOAS instrument – Part 1: Retrieval of 3-D distributions of NO2 and azimuth-dependent OVOC ratios. Atmospheric Measurement Technique, 8, 2371-2395, 2015.

Peters, E., Wittrock, F., GroBmann, K., FrieB, U., Richter, A., Burrows, J.: Formaldehyde and nitrogen dioxide over the remote western Pacific Ocean: SCIAMACHY and GOME-2 validation using ship-based MAX-DOAS observations. Atmospheric Chemistry and Physics. 12 (22), 11179, 2012.

Picornell, M., Ruiz, T., Borge, R. et al. Population dynamics based on mobile phone data to improve air pollution exposure assessments. J Expo Sci Environ Epidemiol 29, 278–291. https://doi.org/10.1038/s41370-018-0058-5, 2019.

Plane, J.M.C., Saiz-Lopez, A.: UV-Visible Differential Optical Absorption Spectroscopy (DOAS). In: Heard, D.E. (Ed.), Analytical Techniques for Atmospheric Measurement. Blackwell Publishing, Oxford, 2006.

Platt, U., Stutz, J.: Differential Optical Absorption Spectroscopy: Principles and Applications. Springer Berlin Heidelberg, Berlin, Heidelberg, Berling, Heidelberg, 2008.

Quaassdorff C, Borge R, Pérez J, Lumbreras J, de la Paz D, de Andrés JM. Microscale traffic simulation and emission estimation in a heavily trafficked roundabout in Madrid (Spain). Sci Total Environ, 566-567:416-427. doi:10.1016/j.scitotenv.2016.05.051, 2016.

Rodgers, C.D.: Inverse Methods for Atmospheric Sounding: Theory and Practice. World Scientific Publishing, Singapore (Singapore), 2000.

Rothman, L.S., Gordon, I.E., Barber, R.J., Dothe, H., Gamache, R.R., Goldman, A., Perevalov, V.L., Tashkum, S.A., Tennyson, J.: HITEMP, the high-temperature molecular spectroscopic database Journal of Quantitative Spectroscopy and Radiative Transfer. 111 (15), 2139, 2150, 2010.

Ryan, R. G., Rhodes, S., Tully, M., Wilson, S., Jones, N., Frieß, U., and Schofield, R.: Daytime HONO, NO_2 and aerosol distributions from MAX-DOAS observations in Melbourne, Atmos. Chem. Phys., 18, 13969–13985, 2018.

Saiz-Lopez, A., Borge, R., Notario, A. et al.: Unexpected increase in the oxidation capacity of the urban atmosphere of Madrid, Spain. Sci Rep 7, 45956. https://doi.org/10.1038/srep45956, 2017.

Schreier, S. F., Richter, A., Peters, E., Ostendorf, M., Schmalwieser, A. W., Weihs, P., & Burrows, J. P: Dual ground-based MAX-DOAS observations in Vienna, Austria:

751 Evaluation of horizontal and temporal NO2, HCHO, and CHOCHO distributions and
752 comparison with independent data sets. Atmospheric Environment: X 5, 2020

753

754 Serdyunchenko, A., Gorshelev, V., Weber, M., Chehade, W., Burrows, J.P.: High
755 spectral resolution ozone absorption cross-sections – Part 2: temperature
756 dependence. Atmospheric Measurement Techniques. 7 (2), 625-636, 2014.

757

758 Solomon, S., & Sanders, Ryan W and Schmeltekopf, A. L.: On the Interpretation of
759 Zenith Sky Absorption Measurements. Journal of Geophysical Research, 92, 8311–
760 8319, 1987.

761

762 Stutz, J., Kim, E.S., Platt, U., Bruno, P., Perrino, C., Febo, A.: UV-visible absorption cross
763 sections of nitrous acid. Journal of Geophysical Research: Atmosphere. 105, 14585-
764 14592, 2000.

765

766 Thalman, R., Volkamer, R.: Temperature dependent absorption cross-sections of O2-
767 O2 collision pairs between 340 and 630 nm and at atmospherically relevant pressure.
768 Physical Chemistry Chemical Physics 15 (37), 15371-15381, 2013.

769

770 Vandaele, A.C., Hermans, C., Simon, P.C., Carleer, M., Colin, R., Fally, S., Mérienne,
771 M.F., Jenouvrier, A., Coquart, B.: Measurements of the NO2 absorption cross-section
772 from 42000 cm^-1 to 10000 cm^-2 (238-1000 nm) at 220 K and 294 K. Journal of
773 Quantitative Spectroscopy and Radiative Transfer; Atmospheric Spectroscopy
774 Application 59 (3), 171-184 96, 1998.

775

776 Volkamer, R., Spietz, P., Burrows, J., Platt, U.: High-resolution absorption cross-section
777 of glyoxal in the UV-vis and IR spectral ranges. J. Photochem. Photobiol. Chem. 172 (1),
778 35-46, 2005.

779

780 Wagner, T., Beirle, S., Benavent, N., Bösch, T., Chan, K. L., Donner, S., Dörner, S., Fayt,
781 C., Frieß, U., García-Nieto, D., Gielen, C., González-Bartolome, D., Gomez, L., Hendrick,
782 F., Henzing, B., Jin, J. L., Lampel, J., Ma, J., Mies, K., Navarro, M., Peters, E., Pinardi, G.,
783 Puentedura, O., Puķīte, J., Remmers, J., Richter, A., Saiz-Lopez, A., Shaiganfar, R.,
784 Sihler, H., Van Roozendael, M., Wang, Y., and Yela, M.: Is a scaling factor required to
785 obtain closure between measured and modelled atmospheric O4 absorptions? An
786 assessment of uncertainties of measurements and radiative transfer simulations for 2
787 selected days during the MAD-CAT campaign. Atmospheric Measurement Techniques
788 12, 2745–2817, 2019.

789

790 Wang, S., Cuevas, C.A., Frieß, U., Saiz-Lopez, A.: MAX-DOAS retrieval of aerosol
791 extinction properties in Madrid, Spain. Atmospheric Measurement Techniques
792 9,5089–5101, 2016.

793

794 World Health Statistics (WHO): monitoring health for the SDGs. Wold Health
795 Organization, 2019.

796

797 Yang, T., Si, F., Luo, Y., Zhan, K., Wang, P., Zhou, H., Zhao, M., & Liu, W.:Source
798 contribution analysis of tropospheric NO_2 based on two-dimensional MAX-DOAS
799 measurements. Atmospheric Environment, 2019.